Monthly Notices of the ROYAL ASTRONOMICAL SOCIETY LETTERS

Mon. Not. R. Astron. Soc. **407,** L89–L93 (2010) doi:10.1111/j.1745-3933.2010.00911.x

Simulation of dark lanes in post-flare supra-arcades – II. A contribution to the remote sensing of the coronal magnetic field

W. Schulz,[1⋆] A. Costa,[1,2,3] S. Elaskar[1,2] and G. Cid[1]

[1] *Facultad de Ciencias Exactas, Físicas y Naturales, Universidad Nacional de Córdoba, Argentina*
[2] *Consejo Nacional de Investigaciones Científicas y Técnicas, CONICET, Argentina*
[3] *Instituto de Astronomía Teórica y Experimental, IATE-CONICET, Argentina*

Accepted 2010 June 25. Received 2010 June 7; in original form 2010 April 21

ABSTRACT

We integrate the MHD ideal equations to simulate dark void sunwardly moving structures in post-flare supra-arcades. In Costa et al. we could numerically reproduce the observations described in Verwichte et al. We showed that the dark tracks are plasma vacuums generated by the bouncing and interfering of shocks and expansion waves, upstream an initial slow magnetoacoustic shock produced by a localized deposition of energy modelled as a pressure perturbation. The same pressure perturbation produces a transverse to the field or perpendicular magnetic shock giving rise to non-linear waves that compose the kink-like plasma void structures, with the same functional sunward decreasing phase speed and period's constancy with height, as those determined by the observations. In this Letter we accomplish a study of sensitivity to initial and background physical conditions of the phenomenon. With the aim of contributing to the remote sensing of the corona we describe the characteristics of different void structures in terms of physical conditions, i.e. magnetic field intensity and pressure perturbation, given a background density.

Key words: magnetic fields – shock waves – Sun: corona.

1 INTRODUCTION

Dark sunward sinuous lanes moving along a fan of rays above post-flare loops towards a supra-arcade have been extensively studied (McKenzie 2000; Innes, McKenzie & Wang 2003a,b; Asai, Yokoyama & Shimojo 2004; McKenzie & Savage 2009). The down moving structures observed at 40–60 Mm heights above the top of arcades, with a decelerating speed in the range of $\sim$50–1000 km s^{-1} were interpreted as sunward voided flows generated by reconnection processes developed by a current sheet above the flare arcade. Other configuration consistent with the observations is a magnetic flux tube, filled with flux and very little plasma, shrinking into the post-eruption arcade (McKenzie & Hudson 1999; McKenzie 2000). Verwichte, Nakariakov & Cooper (2005, hereafter VNC) analysed transverse to the magnetic field oscillations associated with sunward dark lanes in a post-flare supra-arcade. They found that the phase speeds and the displacement amplitudes of observational dark lanes of a kink-like type decrease as they propagate downwards while the period remains constant with height. The phase speeds decrease and periods increase as a function of time.

In Costa et al. (2009, hereafter Paper I), by the integration of the 1D$\frac{1}{2}$ MHD ideal equations, we presented a new scenario to numerically give an account of the observational dark voids described in VNC. We simulated the effects of an initial impulsive and localized deposition of energy – supposed to be associated with the above reconnection processes – in a plasma structured by sunward magnetic field lines. The impulsive phase was modelled by a pressure perturbation that initiates two main different types of processes, a fundamentally hydrodynamic shock pattern directed sunwards and a perpendicular magnetic shock one, i.e. transversal to the magnetic field. The two patterns were supposed to be independent processes however linked by their common origin and background magnetic and density conditions. The independence of the two dynamics was justified due to the far more effective conductive energy transport along field lines than across them. In the transverse direction y, the resulting interactions of non-linear shocks that rebound in the denser external medium composes and sustains, in accordance with observational characteristic times of the phenomenon, a density structure with a central void resembling a kink-like or a sausage-like mode. The same reference values were used as initial conditions to simulate the sunward evolution. We could reproduce the observational data showing that initially two opposite shock-evolving fronts are produced. One evolves towards the Sun's surface until it is absorbed, and the other goes upwards and is forced to rebound resembling the action of the reconnection site. Afterwards, the interaction of upwardly and downwardly moving perturbations forms an expansion wave region that lowers the density of the medium. Also a voided zone is formed and sustained, lasting for times comparable with observational times, due to the continuous interfering of non-linear

⋆E-mail: wschulz@efn.uncor.edu

waves. This evolution, where the magnetic field plays the role of being the wave guide of hydrodynamic shocks (Fernández et al. 2009), reproduces with good accuracy the low speed void observational patterns in VNC. The composition of the two dynamics, the sunward-directed hydrodynamic shock pattern and the perpendicular magnetic one, composes an overall description of a moving transversally shaking void, resembling a kink-like mode as it moves towards the Sun's surface.

This Letter is a continuation of Paper I, and now we analyse the sensibility of the phenomena to different initial conditions and, subject to the limitations of our modelling, we show the functional dependence of the amplitude, the phase speed and the period with the plasma initial quantities. We estimate the range of possible physical conditions that could give rise to the voided phenomena, i.e. magnetic field intensity and triggering pulse pressure.

2 NUMERICAL METHOD AND CALIBRATION

To simulate time-dependent MHD flows we use a method developed by us and described in Paper I.

We perform two $1D\frac{1}{2}$ independent integrations resembling two main initial shock wave fronts triggered by the same pressure perturbation: one directed sunwards, parallel to the field lines, and the other directed transversally to them. The coordinate x represents the sunward direction and the y coordinate the transverse to the magnetic field one, as seen by the line of sight. We chose as test case the edge C observational parameters taken from VNC, shown in Table 1 (N^o : 2). The non-dimensional quantities used for the numerical simulations are the ratios of a dimensional quantity and a reference one. We assume an initial non-perturbed ratio of pressure values, $\beta = 0.1$, and a characteristic background density value as the reference value $\rho_{\rm ref}$. Other reference values are derived from the following calibration iterative procedure based on the transverse shock case.

(i) We chose $B_{\rm ref}$ as the background magnetic field value of the test case. The reference value of the magnetic pressure is $P_{\rm ref} = B_{\rm ref}^2/(2\mu_0)$.

(ii) From the numerical transverse simulation (e.g. Fig. 1a) we obtain $A_{\rm ref}$ and $\tau_{\rm ref}$, $\tau_{\rm ref} = \tau/\tau_n$ and $A_{\rm ref} = A/A_n$, A and τ being the observational values for the amplitude and period of the test case, respectively, in Table 1. A_n and τ_n are the non-dimensional amplitude and period taken from the simulation.

Table 1. Observational wave parameters taken from VNC. τ is the period, $V_{\rm ph}$ is the sunward observational phase speed and A is the amplitude.

N^o	1	2 (test)	3	4	5	6
τ (s)	91	134	182	182	175	217
A (km)	328	906	811	594	246	375
$V_{\rm ph}$(km s^{-1})	220	202	171	218	176	110

Table 2. Initial condition values (1) for the transverse pattern simulation shown in Fig. 1 and (2) for the sunward pattern simulation shown in Fig. 4(c). The initial conditions are $P_1 = P_3$, $\rho_1 = \rho_2 = \rho_3 = 1$, as defined in Paper I.

Edge	y_1, y_2, y_3	$P_2/P_{1,3}$	x_1, x_2, x_3
C(transverse)	0.7, 0.04, 0.26	20	–
C(radial)	–	20	0.7, 0.25, 0.05

(iii) The transverse non-dimensional speed, amplitude and period are related by the expression, $V_n = 2A_n/\tau_n$. The reference speed value for this oscillation is determined from the corresponding dimensional speed $V = V_n V_{\rm ref} = 2A/\tau$ as $V_{\rm ref} = 2A/(\tau V_n)$.

(iv) It is reasonable for the transverse oscillation to relate the reference magnetic field with the Alfvén speed. Thus, if the reference magnetic field satisfies $V_{\rm ref} = B_{\rm ref}/\sqrt{\mu_0\rho_{\rm ref}}$, the iteration finishes. If not, new elections of $B_{\rm ref}$ are accomplished – giving new numerical determinations of A_n, τ_n and V_n – until the relation holds.

Then, the reference temperature value is obtained from the condition $\beta = 0.1$: $P_{\rm gas} = 0.1$, $P_{\rm ref} = k_{\rm B}\rho_{\rm ref}T_{\rm ref}/m_{\rm p}$ ($k_{\rm B}$ and $m_{\rm p}$ are the Boltzmann constant and proton mass, respectively). For $\rho_{\rm ref} = 10^{-12}$ kg m^{-3}, the resulting reference values are $B_{\rm ref} = 8$ G, $P_{\rm ref} = 0.25$ Pa, $T_{\rm ref} = 3 \times 10^6$ K and $V_{\rm ref} = 501$ km s^{-1}. $A_{\rm ref} = 33\,556$ km and $\tau_{\rm ref} = 67$ s correspond to the non-dimensional values $A_n = 0.027$ and $\tau_n = 2$ obtained from Fig. 1(a).

The reference values $\rho_{\rm ref}$, $B_{\rm ref}$, $P_{\rm ref}$, $T_{\rm ref}$ and $\tau_{\rm ref}$ are also used for the sunward simulation. The characteristic radial length is chosen, resembling VNC data, taking into account that the triggering pressure pulse is localized at $L_v = 50$ Mm. We then proceed with the analysis of sensitivity, i.e. varying the sunward magnetic field, B, and the localized deposition of energy, modelled as a pressure perturbation P_2/P_1. P_2 is the triggering pressure pulse localized at the partition y_2 (corresponding to $L_v = 50$ Mm) of the whole interval $y = (y_1, y_2, y_3)$ (see the fig. 1 scheme of Paper I and Table 2). $P_1 = P_3$ is the background gas pressure value of the corona.

Different simulations performed varying the boundary density at the extremes of the integration domain – allowing partial or total rebounds of the waves – showed that the characteristic parameters of the oscillation are slightly changed. Varying the boundary density between the non-dimensional values (4–10), and the partial momentum rebound within (0.25–1), the amplitude and period are not appreciably changed. Thus, we fixed the non-dimensional boundary condition with a density step 5 and a momentum rebound factor of 0.5. This is in accordance with Innes et al. (2003a,b), who estimated that the density values of the oscillating pattern can rise at least between two and five times from the void to the denser medium.

3 RESULTS AND DISCUSSION

3.1 Transverse perpendicular magnetic shocks

Figs 1(a)–(d) display, respectively, the numerical results of the density, temperature, magnetic pressure and gas pressure patterns of the test case as a function of time. The void, which fits the edge C description in VNC, is the result of a non-linear evolution of waves triggered by the instantaneous initial pressure pulse that excites the whole pattern. As in Paper I, we note that the perturbation, seen as a transverse to the field line phenomenon, produces opposite magnetic shock waves that bounce in the lateral and denser boundary medium. The resulting oscillatory pattern of interacting non-linear waves composes a void cavity which is sustained for a time interval that approximately matches the observations. In accordance with McKenzie (2000), Figs 1(a) and (b) show that the moving voids consist of a low-density and high-temperature plasma with respect to the surrounding medium. The density and temperature change, respectively, from about 5×10^{-13} kg m^{-3} and 8×10^6 K inside the void to 10^{-12} kg m^{-3} and 6×10^5 K outside the void. McKenzie & Savage (2009) suggested that the magnetic flux within the voids could provide supporting pressure, due to the ability of the voids to

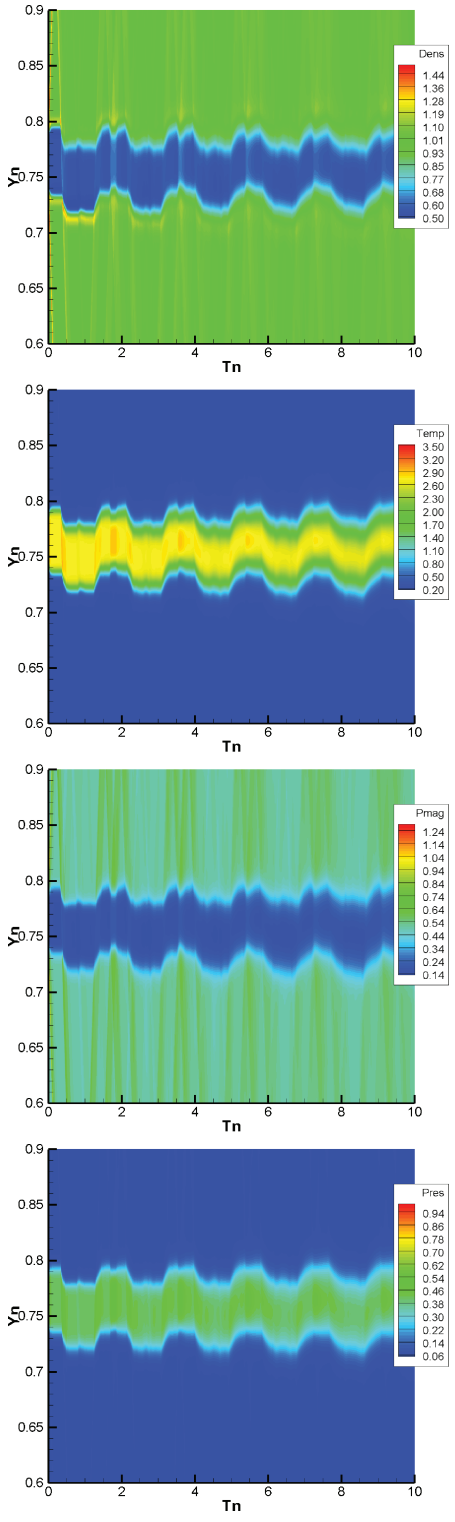

Figure 1. Test case: (a) non-dimensional density; (b) non-dimensional temperature; (c) non-dimensional magnetic pressure; (d) non-dimensional gas pressure. Dimensional values obtained multiplying by $A_{\rm ref} = 33\,556$ km, $\tau_{\rm ref} = 67$ s, $T_{\rm ref} = 3.10^6$ K, $\rho_{\rm ref} = 10^{-12}$ kg m^{-3} and $P_{\rm ref} = 0.25$ Pa.

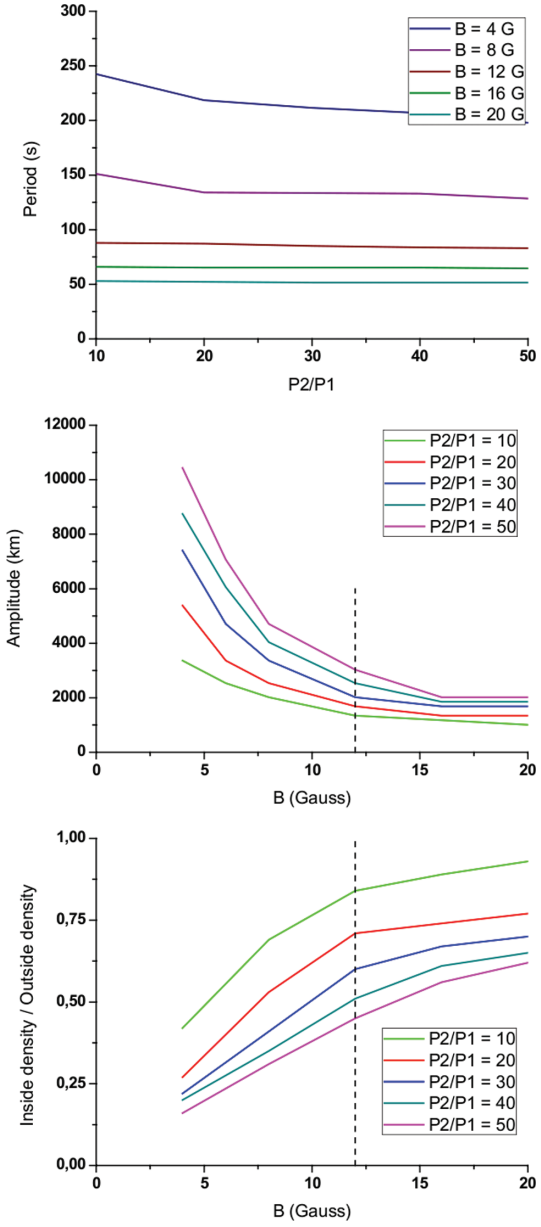

Figure 2. (a) Period versus triggering pulse intensity for different values of the magnetic field. (b) Amplitude of the perturbation pattern versus the magnetic field for different values of the pressure pulse. (c) Void density over outside density versus magnetic field for different values of the pressure pulse.

resist being filled in immediately by the surrounding ambient plasma. Fig. 1(c) shows that the magnetic pressure is lower inside the void than in the external medium. However, due to the larger temperature values inside the void, it results that the inner gas pressure (see Fig. 1d) compensates for the lower magnetic pressure, both of which equilibrate the lower gas pressure plus the larger magnetic pressure of the outside media, e.g. at $(\tau_n, y_n) \approx (0.5, 0.75)$ the total inside pressure $(P_{\rm g} + P_{\rm mag})_{\rm in} \simeq 0.43 + 0.15$, which equals the total outside pressure $(P_{\rm g} + P_{\rm mag})_{\rm out} \simeq 0.05 + 0.54$ at $(\tau_n, y_n) \approx (0.4, 0.8)$. Thus, our simulations allow a description of the phenomenon where the void cavity is a $\beta > 1$ perturbed region obtained as a consequence of the non-linear interaction of transverse waves more than a voided plasma loop magnetically structured. If this argument is right, then the void can be thought of as an emergent property of the collective and non-linear plasma interactions.

We then vary the triggering pulse, P_2/P_1, and the magnetic field intensity B. Fig. 2(a) shows the dependence of the period with the triggering pulse intensity for different values of the magnetic field. Note that, while the intensity of the pulse grows, the period is almost

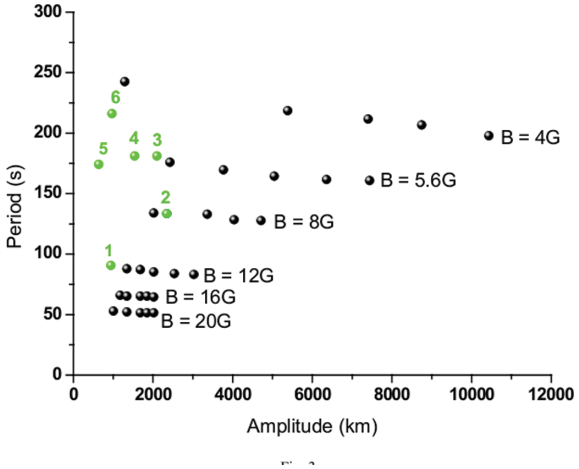

Figure 3. Periods of the numerical simulation (black) and the observational cases in VNC (colour) versus the amplitude.

constant – it varies smoothly for small values of the magnetic field. Beyond $B \simeq 12\,\mathrm{G}$ a small increase of the magnetic field produces a small decrease of the period. On the contrary, below $B \simeq 12\,\mathrm{G}$ a small decrease in the magnetic field produces larger increases of the period. Fig. 2(b) shows the variation of the amplitude with the sunward magnetic field. As in Fig. 2(a), significant variations of the amplitude are found for small values of the magnetic field. The variations are more pronounced for increasing pulse intensities. Beyond $B \simeq 12\,\mathrm{G}$ the amplitude of the void structure is smoothed out, while the magnetic field increases. Fig. 2(c) shows the ratio between the density inside and outside the void as a function of the magnetic field intensity for different values of the pressure pulse. The ratio tends to 1 for vanishing values of the pressure pulse. Again, we note a different behaviour at both sides of $B \simeq 12\,\mathrm{G}$, i.e. the density of the void increases for increasing magnetic field values up to $B \simeq 12\,\mathrm{G}$ and becomes almost constant for larger values than $B \simeq 12\,\mathrm{G}$. If the magnetic field is augmented, as for $B \simeq 32\,\mathrm{G}$, the variation of the density step between its inside and outside values tends to zero.

As it is known from shock wave theory of uniform plasmas (see e.g. Kirk, Melrose & Priest 1994), the Rankine–Hugoniot jump relations establish that the effect of the magnetic field in a perpendicular magnetic shock is to reduce the ratio of densities at both sides of the discontinuity below its hydrodynamic value. Also, the magnetic compression and the maximum density ratio ($X = B_B/B_A = \rho_B/\rho_A$, A and B corresponding to each side of the discontinuity) are limited. For an ideal monotonic gas the range of compression is $1 < X < 4$. From these arguments it could be conjectured that, as in the uniform case, in this context of non-linear interaction of waves and shocks the augmentation of the magnetic field contributes to smooth shock effects in comparison with the hydrodynamic case. The effect is more pronounced when $B \to 32\,\mathrm{G} \sim 4B_{\mathrm{ref}}$, where $\rho_{\mathrm{out}} - \rho_{\mathrm{in}} \to 0$. Beyond a given magnetic field value, e.g. $B \simeq 12\,\mathrm{G}$, the increase of its intensity would lead to the saturation and moderation of the sharp transverse shock wave effects.

Figs 2(a)–(c) suggest a simple relation between the amplitude and the period for large values of the magnetic field. Fig. 3 displays the numerical periods versus the amplitudes. The observational values of the different VNC cases were added in a different colour (see Table 1). Note that all the cases of a given magnetic field are aligned and separated each one from another. The test case, equivalent to N^o : 2 (edge C in VNC) is aligned with the $B \simeq 8\,\mathrm{G}$ cases, N^o : 1 with the $B \simeq 12\,\mathrm{G}$ cases, N^o : 3, 4 and 5 are aligned with the $B \simeq (5\text{–}6)\,\mathrm{G}$ cases and N^o : 6 with the $B \simeq (4\text{–}5)\,\mathrm{G}$ cases.

From the figure, and in the context of a typical initial background density, it can be appreciated that the period is almost a function of the magnetic field only, i.e. $\tau(B)$, while the amplitude is a function of both, the magnetic field and the ratio of pressure pulses, $A(P_2/P_1, B)$. Thus, in the context of our model, given a background density, ρ_{ref}, and assuming a triggering pressure pulse P_2/P_1, we could estimate a background magnetic field from the observational data τ and A. In the next section we show that the pressure pulse can be determined from the observational radial phase speed value, V_{ph}.

3.2 Radial hydrodynamic shocks

In the radial direction the pressure pulse is supposed to be associated with an upward-reconnection event, from where field lines slowly retract away under the force of magnetic tension (McKenzie 2000). The pulse generates shocks travelling sunwards and outwards, along the magnetic field lines. The non-linear interaction of outward rebound waves, near the reconnection site, and sunward absorbed ones compose an overall descending void structure.

Fig. 4 gives numerical results obtained varying the pressure pulse: $P_2/P_1 = 2, 5$ and 20, respectively. In accordance with the assumption that in the radial direction the role of the magnetic field is to guide the interacting hydrodynamic waves, the figures are not modified when the magnetic field intensity is varied. Fig. 4(c), equivalent to fig. 2(c) in VNC, corresponds to the test case. The sunward perturbation is absorbed by the denser media nearer to the Sun's surface, at the location of the void head. The upward-moving shock is forced to rebound at $x_n = 1$. The interaction of the subsequent waves composes a downward-moving void as it is indicated in the figures by the colour contrast, i.e. darker features correspond to lower values of the density. The behaviour of the different cases is similar. The sharpest curves that originate at $x_n = 0.7$, $t_n = 0$, and end at the void head at $x_n = 0$, $t_n \simeq 2.2,\ 1.6,\ 0.8$ in Figs 4(a)–(c), respectively, are the main downward shocks, recognized due to the density enhancement at the shock front, e.g. in Fig. 4(b) for $x_n = 0.2$ the non-dimensional density varies from $\rho_n = 1$ to 2.02. Later interactions compose sunward-moving expansion waves. They are recognized because the density is diminished at its pass. This can be observed in Fig. 4(c) at $x_n = 0.4$; the density diminishes, after the shock, from $\rho_n = 3.3$ at $t_n \sim 0.34$ to $\rho_n = 2.0$ at $t_n \sim 0.47$. The whole interacting pattern generates a region that is separated from a vacuum upper zone, also formed by the interaction of non-linear upward- and downward-moving perturbations. This vacuum zone can be clearly appreciated in Fig. 4. The density of the vacuum zone is more pronounced depending on the larger pressure ratio values ($P2/P1$), e.g. for $x_n = 0.8$ and $t_n = 1.8$ in Figs 4(a)–(c) the density values are, respectively, 0.64, 0.44 and 0.25.

It is interesting to note the similarity between the numerical results and figs 2(c) and (d) in VNC. From the figures in VNC and our Figs 4(a) and (b) it can be appreciated that pronounced slope curves at the beginning of the event resemble shock waves leading to a posterior augmentation of the density. Later the formation of a denser, smooth and extended region with a neighbouring vacuum zone that lasts over time resembles the interaction wave pattern of our numerical description.

To compare our sunward speed values with those in VNC we calculated the speed of the curve limiting the vacuum zone. The VNC curve was obtained as in Paper I. Fig. 5 shows the good accordance between the test numerical case and the corresponding observational curve. The value $V_{\mathrm{ph}} = 202\,\mathrm{km\,s^{-1}}$, the speed mea-

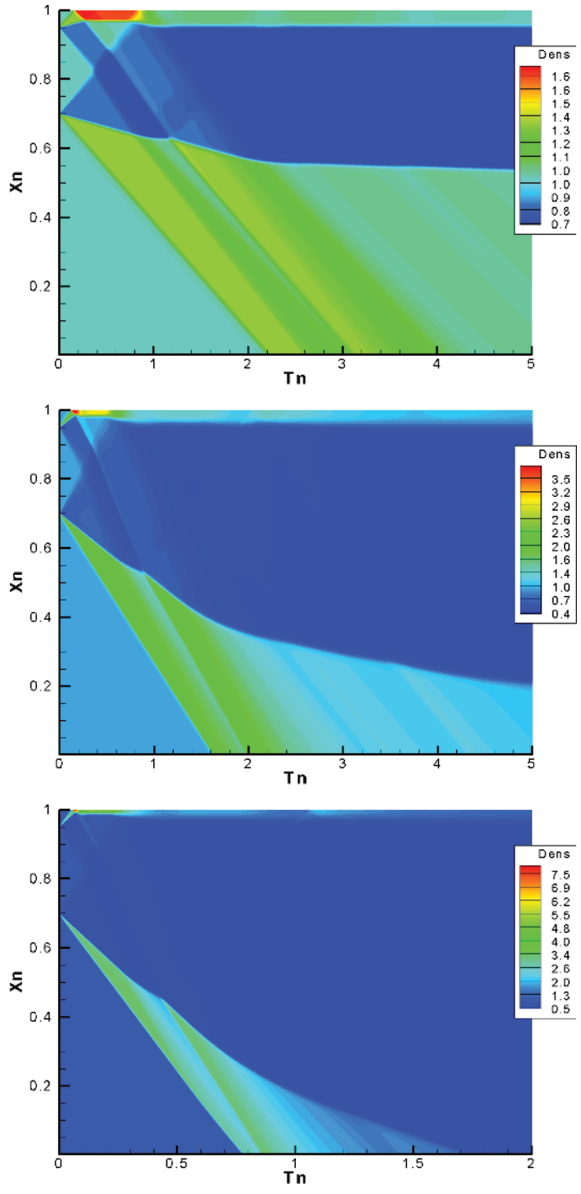

Figure 4. Radial simulation for P_2/P_1 equals to (a) 2, (b) 5 and (c) 20 (test), respectively. $x_n = 0.7$ corresponds to $L_v = 50$ Mm, the characteristic length of the phase speed sunward variation in VNC.

sured by VNC at x_0, corresponds to the simulation speed at the origin of coordinates. By simple inspection of Figs 4(a) and (b) we note that their phase speed curves differ appreciably from the test, Fig. 4(c), and observational cases. Figs 4(a)–(c) correspond to different values of P_2/P_1 and are independent of the magnetic field intensity, however, linked to $B_{\rm ref}$ via the relation $P_1 < P_{\rm ref}$. Thus, the fact that Fig. 5 matches the observations means that $P_2/P_1 = 20$ is a good estimation of the triggering pulse leading to the test-case phenomenon. If the matching is not good enough, the whole process has to begin again.

4 SUMMARY AND CONCLUSIONS

We numerically reproduce dark lane moving phenomena observationally detected in post-flare supra-arcades. We showed that the dark tracks are consistent with plasma vacuums generated by the bouncing and interfering of shocks and expansion waves, upstream an initial localized deposition of energy which is responsible for two

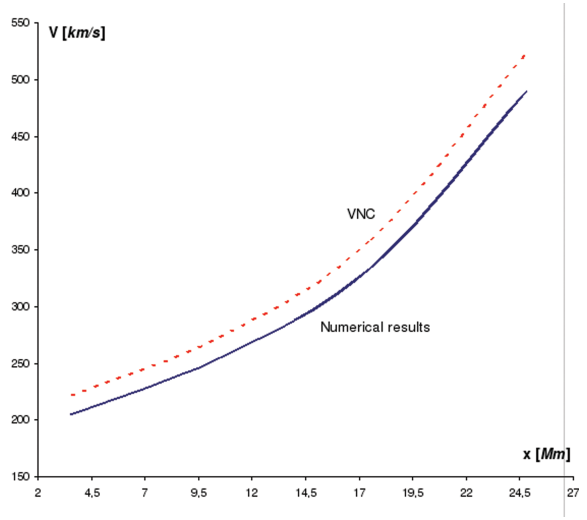

Figure 5. Radial speed for the numerical cases and edge C case in VNC versus the sunward distance.

dynamics. The composition of both, a resulting sunward-directed hydrodynamic shock pattern and a perpendicular magnetic shock one, composes an overall $\beta > 1$ transversally shaking void moving towards the Sun's surface, which resembles the kink-like mode described in VNC.

From the transverse simulation we found that, in accordance with the shock wave theory of uniform media, there is a critical value of the magnetic field beyond which the behaviour of the magnetic shock pattern changes, the magnetic compression is limited and the phenomenon is progressively saturated. We also found that the period of the kink-like structure is a function of the magnetic field intensity only, while the amplitude is a function of both, the magnetic field intensity and the triggering pressure pulse. Thus, the period's constancy with height found in VNC can be associated with the almost constancy with height of the background magnetic field in the region. Consequently, the variation of the amplitude with height will be determined by the distance from the triggering pulse.

In accordance with our interpretation that in the sunward direction the magnetic field plays the role of being a waveguide, the pressure pulse determines a hydrodynamic shock that moves towards the Sun's surface at slow acoustic speed values and the dynamics is independent of the magnetic field intensity. From the period, the amplitude and the sunward phase speed of the observational kink-like phenomenon, given a characteristic background density value, we estimated, in the frame of our model, the magnetic field and the triggering pressure pulse.

REFERENCES

Asai A., Yokoyama T., Shimojo M., 2004, ApJ, 605, L77
Costa A., Elaskar S., Fernández C., Martínez G., 2009, MNRAS, 400, L85 (Paper I)
Fernández C., Costa A., Elaskar S., Schulz W., 2009, MNRAS, 400, 1821
Innes D. E., McKenzie D., Wang T., 2003a, Sol. Phys., 217, 247
Innes D. E., McKenzie D., Wang T., 2003b, Sol. Phys., 217, 267
Kirk J., Melrose D., Priest E., 1994, Plasma Astrophysics. Springer-Verlag, Berlin
McKenzie D., 2000, Sol. Phys., 195, 381
McKenzie D., Hudson H., 1999, ApJ, 519, L93
McKenzie D., Savage S., 2009, ApJ, 697, 1569
Verwichte E., Nakariakov V., Cooper F., 2005, A&A, 430, L65 (VNC)

This paper has been typeset from a TEX/LATEX file prepared by the author.